Journal of Cerebral Blood Flow & Metabolism (2010) 30, 1598–1607

www.jcbfm.com

MRI estimation of global brain oxygen consumption rate

Varsha Jain, Michael C Langham and Felix W Wehrli

Laboratory for Structural NMR Imaging, Department of Radiology, University of Pennsylvania Medical Center, Philadelphia, Pennsylvania, USA

Measuring the global cerebral metabolic rate of oxygen ($CMRO_2$) is a valuable tool for assessing brain vitality and function. Measurement of blood oxygen saturation (HbO_2) and flow in the major cerebral outflow and inflow vessels can provide a global estimate of $CMRO_2$. We demonstrate a rapid noninvasive method for quantifying $CMRO_2$ by simultaneously measuring venous oxygen saturation in the superior sagittal sinus with magnetic resonance susceptometry-based oximetry, a technique that exploits the intrinsic susceptibility of deoxygenated hemoglobin, and the average blood inflow rate with phase-contrast magnetic resonance imaging. The average venous HbO_2, cerebral blood flow, and global $CMRO_2$ values in eight healthy, normal study subjects were 64% ± 4%, 45.2 ± 3.2 mL per 100 g per minute, and 127 ± 7 μmol per 100 g per minute, respectively. These values are in good agreement with those reported in literature. The technique described is noninvasive, robust, and reproducible for *in vivo* applications, making it ideal for use in clinical settings for assessing the pathologies associated with dysregulation of cerebral metabolism. In addition, the short acquisition time (~30 seconds) makes the technique suitable for studying the temporal variations in $CMRO_2$ in response to physiologic challenges.
Journal of Cerebral Blood Flow & Metabolism (2010) **30,** 1598–1607; doi:10.1038/jcbfm.2010.49; published online 21 April 2010

Keywords: cerebral blood flow measurement; cerebral oxygen metabolism; MR susceptometry; oxygen saturation; phase-contrast MRI

Introduction

Under normal physiologic conditions, aerobic metabolism of glucose is the primary metabolic fuel for energy production in the human brain (Greene *et al*, 2003; Lowry *et al*, 1964). Although the brain represents only 2% of the body weight, it receives 15% of the cardiac output and consumes 20% of the total body oxygen (Magistretti and Pellerin, 1996; Quastel and Wheatley, 1932). The above highlights the critical dependence of brain function on continuous, efficient usage of oxygen, and the organ's heightened vulnerability and sensitivity to alterations in oxygen supply. There is a considerable body of research exploring the dysregulation of glucose oxidative metabolism in diseases of the brain. Many of the most common disorders of the brain, such as Alzheimer's, Parkinson's, Huntington's, multiple system disorder, progressive supranuclear palsy, mitochondrial encephalomyopathy, and others, have been found to be associated with alterations in cerebral oxygen metabolism (Ishii *et al*, 1996; Leenders *et al*, 1986; Santens *et al*, 1997; Shishido *et al*, 1996; Tanaka *et al*, 1997). In addition, a measure for assessing the cerebral metabolic rate of oxygen ($CMRO_2$) consumption will further enhance our understanding of normal cerebral physiology during rest, sleep, anesthesia, aging, functional brain tasks, and physiologic challenges, as well as be useful for evaluating the effect of systemic disease processes such as hypertension and diabetes on cerebral oxygen metabolism. Thus, a robust and reliable measure for quantifying $CMRO_2$ would serve as an important tool for exploring the neuro-metabolic–hemodynamic relationships during cerebral activation and pathophysiologic conditions.

Currently, $CMRO_2$ is not routinely measured clinically, in that several practical limitations have prevented its widespread application. Positron emission tomography provides the most direct measurement of $CMRO_2$ through imaging of the accumulated inhaled ^{15}O-labeled radiotracers in the brain, which, after distribution into the tissue, are converted into ^{15}O-labeled water (Ito *et al*, 2005; Mintun *et al*, 1984). Positron emission tomography is, however,

Correspondence: Dr FW Wehrli, Laboratory for Structural NMR Imaging, Department of Radiology, University of Pennsylvania Medical Center, 1 Founders Building, MRI Education Center, 3400 Spruce Street, Philadelphia, PA 19104, USA.
E-mail: wehrli@mail.med.upenn.edu
This work was supported by grants NIH R01-MH080892 and NIH R21-HL088182.
Received 25 November 2009; revised 5 March 2010; accepted 16 March 2010; published online 21 April 2010

restrictive in terms of its utility because of the high radiation dose, relatively complex setup required for the constant delivery of radio-labeled gases, high associated expenses, and long scan times, during which it is assumed that no change in physiologic state occurs.

Other methods for quantifying $CMRO_2$ have relied on estimating venous oxygen saturation levels using jugular vein oximetry involving catheterization and measuring flow through optical measurements or Doppler ultrasound (Mayberg and Lam, 1996). However, because of the invasiveness of the technique, it is prone to complications such as carotid artery puncture (incidence 1% to 4.5%), hematoma formation, jugular vein occlusion, thrombosis, risk of bacteremia, and other infections (Coplin *et al*, 1997). In addition, the accuracy of the method is highly dependent on personnel skill and experience.

In a recent paper, a magnetic resonance imaging (MRI) approach for quantifying $CMRO_2$, based on the measurement of transverse relaxation time T2 (Wright *et al*, 1991), has been described (Xu *et al*, 2009). The method, termed T2-relaxation-under-spin-tagging (Lu and Ge, 2008), allows noninvasive estimates of venous oxygen saturation *in vivo*. However, T2-based methods rely on an *in vitro* calibration curve to translate T2 measurements to venous oxygen saturation levels (Wright *et al*, 1991). In addition, an acquisition time of over 4 minutes limits the utility of this technique for obtaining time-resolved $CMRO_2$ measurements, as would be desirable to study the effect of physiologic challenges and functional tasks on the global rate of oxygen consumption.

In this study, we present a rapid noninvasive method for quantifying $CMRO_2$. The method comprises simultaneous estimation of oxygen saturation and cerebral blood flow (*CBF*) in the major vessels draining and feeding the brain. Specifically, venous blood oxygen saturation is estimated using susceptometry-based oximetry (Fernandez-Seara *et al*, 2006; Haacke *et al*, 1997), which quantifies the intravascular bulk magnetic susceptibility relative to the surrounding tissue by exploiting the inherent paramagnetism of deoxyhemoglobin in erythrocytes. The blood flow is quantified in the major inflow vessels (internal carotid arteries and vertebral arteries) using phase-contrast MRI (Bryant *et al*, 1984; Dumoulin and Hart, 1986).

Materials and Methods

Estimation of the Cerebral Metabolic Rate of Oxygen Consumption

The cerebral metabolic rate of oxygen can be estimated by combining venous and arterial oxygen saturation and *CBF* measurements using Fick's principle (Kety and Schmidt, 1948),

$$CMRO_2 = C_a CBF(S_aO_2 - S_vO_2) \quad (1)$$

where $CMRO_2$ is the cerebral metabolic rate of oxygen consumption in μmol/minute per 100 g, *CBF* is the total cerebral blood inflow to the brain in mL per 100 g per minute, S_aO_2 and S_vO_2 represent the arterial and venous oxygen saturation levels, respectively, C_a is the oxygen concentration in moles of O_2 per 100 mL of blood. On the basis of a typical hemoglobin level of 14.7 g/dL (at a hematocrit (*Hct*) of 0.42) and an O_2 carrying capacity of 1.39 mL of O_2 per gram of hemoglobin (West, 2007), using the ideal gas law, C_a was calculated to be 836 μmol O_2 per 100 mL blood. For our $CMRO_2$ measurements, an arterial oxygen saturation value of 98% was assumed. This is a valid assumption for normal healthy adults under resting conditions, in whom arterial blood is almost fully oxygenated (West, 2007). S_vO_2 was estimated by magnetic resonance blood oximetry. We note that, in principle, blood oximetry can be used to estimate S_aO_2 as well. However, this measurement of cerebral arterial supply is challenging as the presence of the oropharynx or trachea in the neck causes severe susceptibility-induced magnetic field perturbations, making the S_aO_2 measurement in the internal carotid and vertebral arteries difficult. The measurement in the distal cerebral arterial vasculature (such as the middle cerebral artery) is hampered by constraints such as vessel tortuosity, orientation with respect to B_o field, and small-vessel diameter ($\sim$2 mm). The flow rate was quantified with a nongated phase-contrast MRI technique (Bryant *et al*, 1984; Dumoulin and Hart, 1986; see below).

Principles of Magnetic Resonance Blood Oximetry

Magnetic resonance susceptometry-based oximetry (Fernandez-Seara *et al*, 2006; Haacke *et al*, 1997) relies on the magnetic susceptibility difference $\Delta\chi$ between intravascular blood and surrounding tissue. By modeling the blood vessel as a long paramagnetic cylinder, an exact expression for the incremental field ΔB can be derived as (Schenck, 1996)

$$\Delta B = 1/6\,\Delta\chi\, B_0\,(3\,cos^2\theta - 1) \quad (2)$$

ΔB is measured from a phase difference image that yields $\phi(TE_1) - \phi(TE_2) = \gamma \Delta B \Delta TE$, where ΔTE is the interecho spacing between two gradient-recalled echoes. For whole blood

$$\Delta\chi = \chi_{do} Hct(1 - HbO_2) \quad (3)$$

where $\Delta\chi_{do} = 4\pi \cdot 0.27$ p.p.m. (Spees *et al*, 2001) is the susceptibility difference in SI units between fully deoxygenated and fully oxygenated erythrocytes, HbO_2 is the fraction of the oxygenated hemoglobin, *Hct* is the volume fraction of the packed erythrocytes in whole blood, and θ is the tilt angle of the vessel with respect to the main field B_o. It is noted that various values of $\Delta\chi_{do}$ (Thulbourn *et al*, 1982; Weisskoff *et al*, 1992; Plyavin *et al*, 1983) have been reported earlier. We have particular confidence in the value reported by Spees *et al* based on their thorough work, agreement with two different approaches, and a semitheoretical analysis. Thus, HbO_2 can be determined by combining equations (2) and (3) as

$$\%HbO_2 = \left[1 - \frac{2|\Delta\phi|}{\gamma \Delta\chi_{do} B_o (\cos^2\theta - 1/3) Hct}\right] \times 100 \quad (4)$$

where $\Delta\phi$ is the average phase difference between intravascular blood and the surrounding tissue.

Magnetic Resonance Flow Quantification

The flow rate was quantified with a phase-contrast technique (Bryant *et al*, 1984; Dumoulin and Hart, 1986). In the implementation used, the imaging pulse sequence is played out twice in an interleaved manner. In both the acquisitions, the zeroth gradient moment for the slice-selection gradient (i.e., the gradient parallel to the direction of flow) is 0, as usual; thus, the signal from stationary tissue protons is nulled on subtraction of the two datasets. The first gradient moment ($M_1 = \int G(t)t\,dt$) of the two interleaves, which determines the sensitivity of the measured phase difference, $\Delta\varphi$, accrued by the flowing spins, is given as

$$\Delta\varphi = \gamma \Delta M_1 v \quad (5)$$

where ΔM_1 is the difference in first moment between the two interleaves. It is convenient to introduce the parameter VENC (Velocity ENCoding) (Pelc *et al*, 1994), which is the velocity causing a phase shift of π radians. In this manner, equation (5) can be rewritten as

$$\Delta\varphi = \pi \cdot v/VENC \quad (6)$$

from which the blood flow velocity is determined pixel by pixel. It should be noted that the maximum velocity measured should not exceed the user-defined parameter VENC to avoid phase aliasing.

Magnetic Resonance Imaging Protocol

Magnetic resonance experiments were performed on a 3-T Siemens TIM Trio system using vendor-supplied head and neck coils. An interleaved 2D gradient-recalled echo sequence programmed in SequenceTree (Magland and Wehrli, 2006), shown in Figure 1, was used to obtain simultaneous oxygen saturation and *CBF* measurements. The sequence consisted of four interleaves (Figure 1). All but the fourth interleave ($VENC = 60$ cm/s) were flow compensated (i.e., the slice-selection gradient structure was chosen such that $M_1 = 0$) and the interleaves alternated between making the acquisition at the level of the superior sagittal sinus (SSS) and mouth orifice to measure oxygen saturation and total cerebral inflow, respectively. The first and the third interleaves with an echo time (TE) of 7.025 and (7.025 + 2.5) milliseconds (interecho time, $\Delta TE = 2.5$ milliseconds), respectively, were acquired at the level of SSS in the occipital region for blood oxygenation quantification. This interleaved acquisition scheme allowed us to attain short interecho times, thereby avoiding phase wrapping. The second and fourth interleaves were acquired with the same echo time (7.025 milliseconds) at the level of the mouth orifice and were used to quantify the average velocity. For the static phantom experiments, all interleaves were acquired at the same axial location and the data from the first and third interleaves were used for estimation of susceptibility relative to distilled water.

The scan parameters used were as follows: $FOV = 208 \times 208 \times 5\,mm^3$, voxel size = $1 \times 1 \times 5\,mm^3$, dwell time = 15 μs, flip angle = 25°, $VENC = 60$ cm/second, repetition time (TR) = 30 milliseconds, yielding a total scan time of 28 seconds. In addition, a high-resolution scan at the level of the mouth orifice over the same slice as chosen above (voxel size = $0.5 \times 0.5 \times 5\,mm^3$, $FOV = 208 \times 208 \times 5\,mm^3$) was obtained to improve the accuracy of estimation of the vessel cross-sectional area.

The location of the SSS was prescribed based on a sagittal image (Figure 4A). A multislice axial localizer was used to choose a slice with a relatively straight section of SSS based on the observation of a relatively constant spatial position and cross-section of the vessel. The imaging slice was oriented axially, intersecting the SSS at

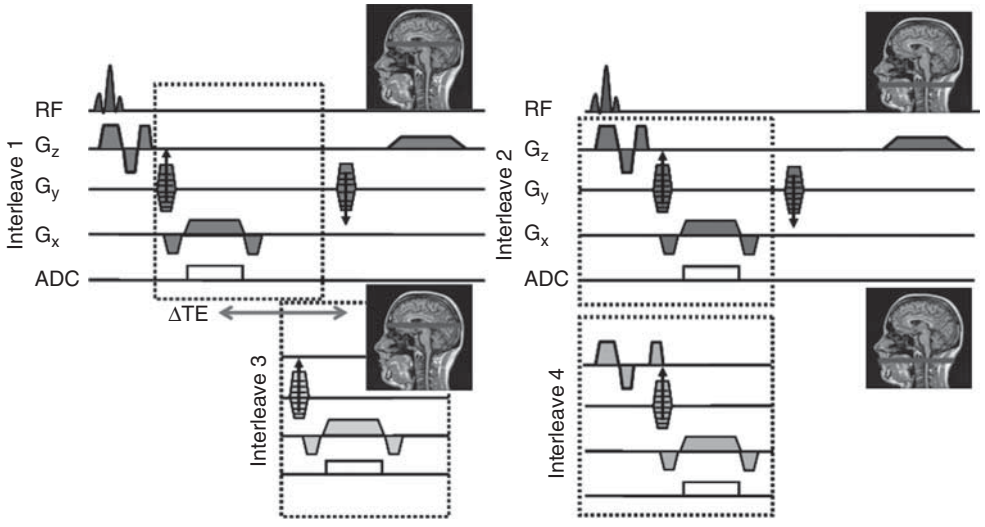

Figure 1 Interleaved 2D gradient-recalled echo sequence alternating between the two anatomic locations (Gx = frequency-encoding gradient, Gy = phase-encoding gradient, Gz = slice-selection gradient). All but the fourth interleave are flow compensated along the slice-select direction. The fourth interleave is flow encoded with a Velocity ENCoding (VENC) = 60 cm/second. The echo time difference (ΔTE) between the first and third interleaves is 2.5 milliseconds (TE = 7.025 milliseconds). The dashed boxes represent sequence parameters that changed between the interleaves.

about 1 to 2 cm above the confluence of sinuses (location at which the inferior sagittal, straight, and transverse sinuses join the SSS). For the prescription of an appropriate slice for flow imaging, it is noted that the anatomic courses of the internal carotid and vertebral arteries before the second cervical vertebra are both nearly parallel to the scanner's z axis. This parallel linear segment is variable in length because of individual differences in the location of the common carotid bifurcation, but is generally a few centimeters in length. A multislice axial localizer was used to identify this segment in the region of the oropharynx, based on the observation of a relatively constant in-plane position and cross-section of the vessel, as it is at the same axial location as the second and third cervical vertebrae.

In addition, we acquired a T_1-weighted 3D magnetization-prepared rapid gradient-echo (MPRAGE; Mugler and Brookeman, 1990) image dataset (voxel size = $1 \times 1 \times 1\,mm^3$) to estimate the intracranial volume in each subject, so that the $CMRO_2$ levels could be calculated per 100 g of brain mass. An average brain density of 1.05 g/mL was used for the above calculation (Kretschmann *et al*, 1986).

The times taken for various scans were 1:12 minutes for the multislice localizer, 28 seconds for the 2D gradient-recalled echo for simultaneous oxygen saturation and flow measurements, 1:37 minutes for T_1-MPRAGE, summing to a total scan duration of 3:17 minutes for whole brain global $CMRO_2$ estimation.

Rationale for Cerebral Metabolic Rate of Oxygen Measurement Locations

The SSS was preferred over the internal jugular vein (another major draining vein) in light of the often severe susceptibility artifacts caused by the proximity of air spaces such as the oral cavity and trachea. In addition, Xu *et al* (2009) have previously shown that the oxygen saturation levels in the SSS are comparable to those in the internal jugular vein. Phase measurement in the SSS is convenient and robust in the absence of major tissue interfaces with markedly different susceptibilities.

Blood flow rates were measured at the neck level in the four feeding vessels, the left and right internal carotid, and vertebral arteries. These vessels run parallel to the neck and the spine, respectively, and the chosen axial slice was perpendicular to the vessels and B_o. Total *CBF* was quantified by measuring inflow instead of outflow, as besides the internal jugular vein, certain secondary vessels such as the vertebral venous plexi also drain the brain (Cooper, 1960); the flow measurement in these vessels is challenging.

Phantom Experiments

The blood vessel of interest (SSS) was modeled as a long circular cylinder (Fernandez-Seara *et al*, 2006; Haacke *et al*, 1997). The SSS runs in the sagittal grove from the anterior to posterior head, tucked between the two cerebral cortices. As a result, the vessel has a triangular (rather than a circular) cross-section. To ensure the applicability of the previously validated model, a phantom was constructed. It consisted of two 12-cm-long tubes, with a circular and triangular cross-section, filled with paramagnetic gadolinium-doped distilled water. The tubes were immersed in the center of a cylindrical plastic container filled with distilled water, with the tubes oriented parallel to the container's long axis. The concentrations of Gd-DTPA in the solutions were 1, 1.25, 1.5, and 1.75 mmol/L so as to cover a range of relative magnetic susceptibilities matching the expected range of susceptibility differences found between partially deoxygenated blood and tissue. The concentrations chosen corresponded to oxygen saturation values between 58% and 76% (assuming an *Hct* of 0.42).

In Vivo Estimation of Cerebral Metabolic Rate of Oxygen

The human subject studies were approved by the Institutional Review Board of the University of Pennsylvania and informed written consent was obtained from each volunteer. Eight healthy male volunteers participated in the study (mean age 25 years; s.d. 5 years). The $CMRO_2$ measurement was repeated three times in each volunteer at intervals of 5 to 10 minutes. In each session, three consecutive measurements were obtained to estimate the mean and standard deviation of each parameter for each session. The subject was asked to rise from the scanner table between each of the three scanning sessions. A cushioned head stabilizer was used to minimize motion and the subject was instructed to stay alert during the course of the scans as $CMRO_2$ measurements are known to be affected by degree of mental alertness.

Data Analysis

For HbO_2 quantification phase maps were obtained, computed as the phase difference between echoes through

$$\Delta\phi = \arg(Z_2 Z_1^*) \tag{7}$$

where Z_1 and Z_2 represent complex values of a particular pixel in the images of two echoes, respectively; the asterisk denotes complex conjugate. The susceptibility difference between air and tissue compartments causes field inhomogeneity, resulting in low spatial-frequency modulation of the phase signal. To reduce its effect, a retrospective correction method was implemented, which approximates the field inhomogeneity with a second-order polynomial, after appropriately masking and weighting the phase image with the corresponding masked magnitude image (Langham *et al*, 2009*a*). To estimate the susceptibility values, the average phase difference between the region of interest and the neighboring area (adjacent water in the phantom experiments and tissue for *in vivo* studies) was calculated. It should be noted that at the investigated field strength, the phase difference images acquired at relatively short *TE*s are not sensitive to the white and gray matter boundaries (Abduljalil *et al*, 2003) as shown in Figure 4D. The background brain parenchyma was also used as reference

tissue in a study using a similar method for quantifying oxygen saturation in pial veins (Haacke *et al*, 1997).

For the quantification of total cerebral blood flow, a signal intensity threshold was applied to the high-resolution magnitude image to obtain a mask for each of the four vessels of interest (internal carotid and vertebral arteries) for measuring the cross-sectional area. The mask was then downscaled to match the resolution of the phase-contrast image and applied to the velocity maps to obtain the whole-brain cerebral blood velocity in mL/minute. Total brain volume was estimated using a semiautomated region growing algorithm in ITKSnap (Yushkevich *et al*, 2006). Analysis of variance was used to test intersubject variability of various test parameters. Within-subject coefficient of variation and intraclass correlation coefficient were used to test technique reproducibility. In addition, the correlation between the arterio-venous oxygen saturation difference ($AVO_2D = S_aO_2 - S_vO_2$) and global *CBF* was analyzed. The above were performed using JMP Statistical Software Package 7.0 (SAS, Cary, NC, USA).

Results

Phantom Experiments

Figure 2 shows the phase difference images of the four phantom experiments. The relative mean difference between the susceptibility values derived from the phase measurements in the circular and triangular cross-section phantoms was 2.6%, which would correspond to an average absolute difference in oxygen saturation of 0.8% at a *Hct* of 0.42 (Table 1).

In Vivo Studies

Magnitude and velocity images for the estimation of the whole-brain *CBF* are showed in Figure 3. Figure 4 shows the magnitude and phase difference images acquired at the level of the SSS used for the

Table 1 The difference in oxygen saturation between the circular and triangular phantom tubes for various concentrations of Gd (assuming $Hct = 0.42$)

[Gd] (mmol/L)	*ΔOx-Sat (%)*
1	1.08
1.25	0.08
1.5	0.75
1.75	1.19

Gd, Gadolinium; Hct, hematocrit; Ox-Sat, Oxygen Saturation.
Summary data from the triangular phantom study.

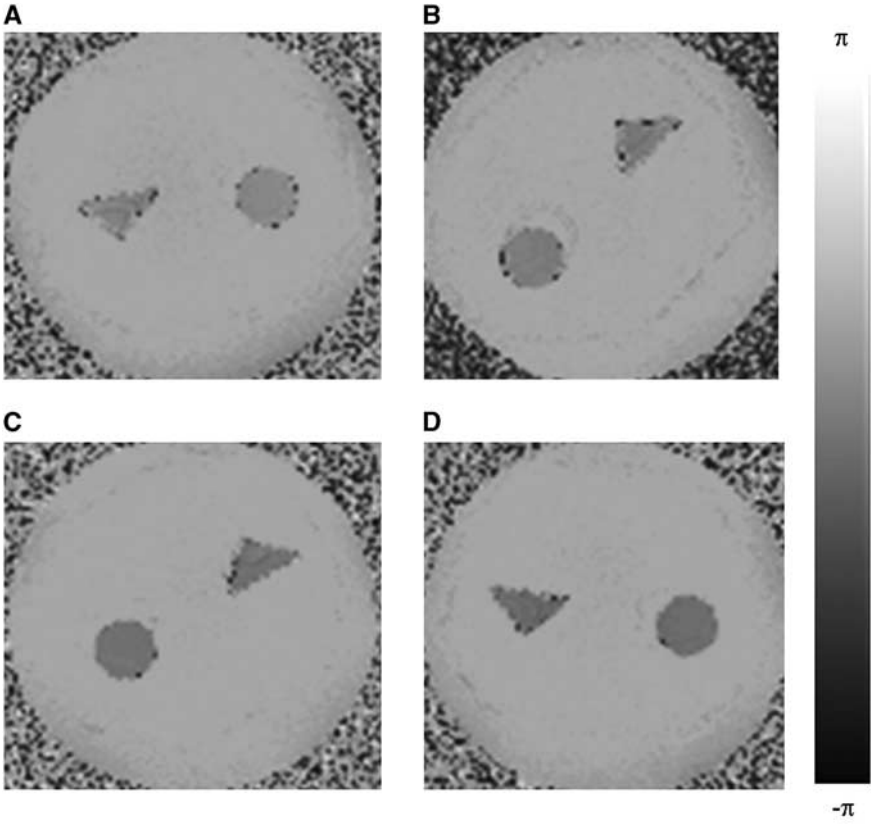

Figure 2 Phase-difference images of the cross-sectional area of the phantoms containing (**A**) 1 mmol/L, (**B**) 1.25 mmol/L, (**C**) 1.5 mmol/L, and (**D**) 1.75 mmol/L Gd-DTPA in distilled water.

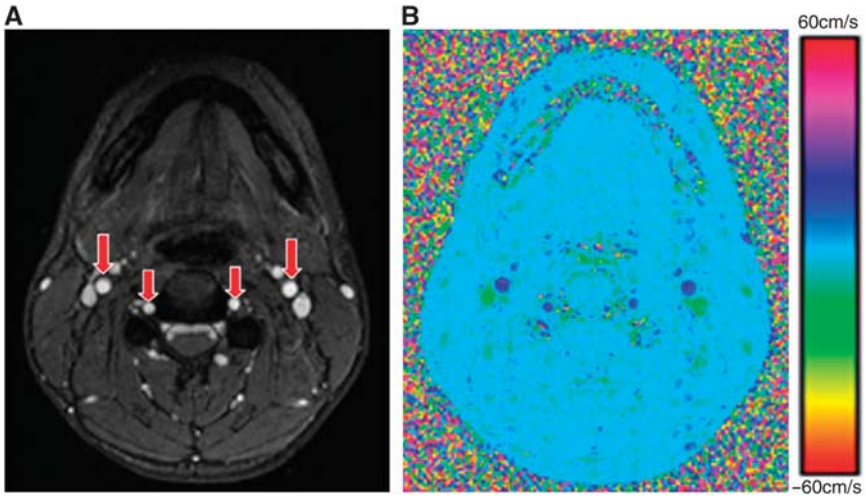

Figure 3 (**A**) Axial magnitude image of mouth orifice highlighting the major inflow vessels (internal carotid and vertebral arteries; red arrows); (**B**) corresponding velocity map used for the calculation of total cerebral blood flow rate.

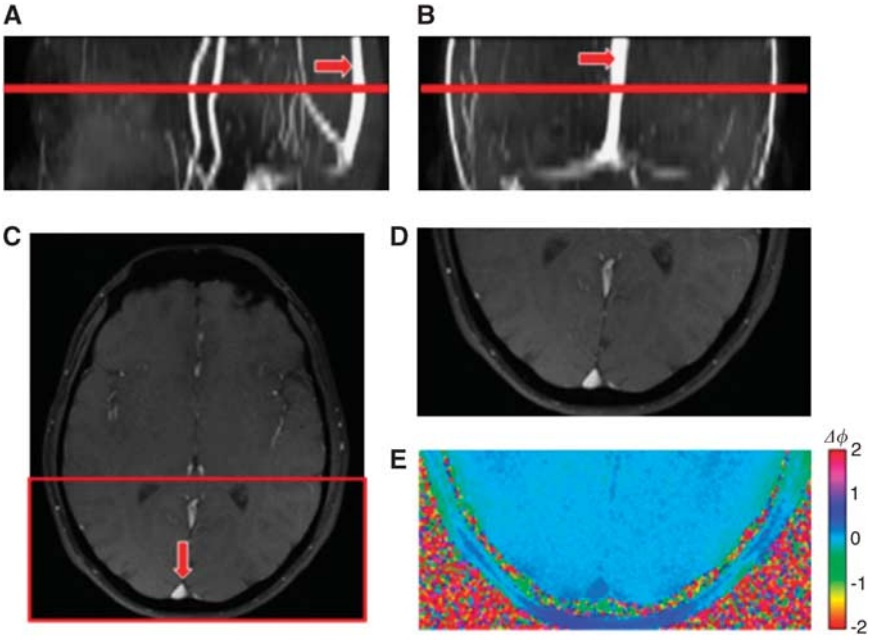

Figure 4 (**A**) Sagittal, (**B**) coronal, and (**C**) axial magnitude images of the brain highlighting the superior sagittal sinus (red arrow). Note that the sinus is fairly straight; the highlighted red line represents the imaging slice location. Zoomed in axial (**D**) magnitude and (**E**) phase image of the superior sagittal sinus.

estimation of oxygen saturation. The average values of venous oxygen saturation and *CBF* for the group of eight subjects were 64% ± 4% and 45.2 ± 3.2 mL per 100 g per minute, respectively. The mean $CMRO_2$ value found was 127 ± 7 μmol per 100 g per minute. The results of the reproducibility test performed in eight subjects are summarized in Table 2. The oxygen saturation and flow measurements in the three sessions varied maximally by 2% HbO_2 and 2.3 mL per 100 g per minute, respectively. The maximal variation in $CMRO_2$ over the three sessions for the group was 8 μmol per 100 g per minute. Figure 5A shows a scatter plot of the mean $CMRO_2$ values computed for each subject for the three scanning sessions. The coefficients of variation for $CMRO_2$, venous oxygen saturation, and *CBF* measurements were 3.2%, 2.3%, and 3.1%, and the intraclass coefficients were 0.94, 0.98, and 0.97, respectively. The AVO_2D was found to be negatively correlated with global *CBF* across the subjects ($R^2 = 0.74$, $P < 0.006$), with large AVO_2D corresponding to low global *CBF* values (Figure 5B).

Table 2 Estimated total cerebral blood flow (*CBF*), venous oxygen saturation in superior sagittal sinus (S_vO_2), and cerebral metabolic rate of oxygen ($CMRO_2$) levels in eight subjects evaluated in three successive sessions to show short-term reproducibility

	Session 1			*Session 2*			*Session 3*		
Subject	CBF *(mL per 100 g per minute)*	S_vO_2 *(%)*	$CMRO_2$ *(μmol per 100 g per minute)*	CBF *(mL per 100 g per minute)*	S_vO_2 *(%)*	$CMRO_2$ *(μmol per 100 g per minute)*	CBF *(mL per 100 g per minute)*	S_vO_2 *(%)*	$CMRO_2$ *(μmol per 100 g per minute)*
1	44.4 ± 1.2	65 ± 1	123 ± 4	45.1 ± 1.0	64 ± 1	129 ± 5	45.4 ± 0.7	64 ± 1	129 ± 4
2	42.4 ± 1.7	64 ± 2	119 ± 5	41.0 ± 1.3	63 ± 2	118 ± 2	41.4 ± 0.7	63 ± 1	120 ± 3
3	52.4 ± 1.1	71 ± 1	118 ± 4	50.8 ± 1.1	71 ± 2	114 ± 4	50.7 ± 1.3	70 ± 1	116 ± 3
4	47.3 ± 1.3	66 ± 2	127 ± 6	48.2 ± 0.6	65 ± 1	131 ± 7	48.3 ± 1.3	67 ± 2	123 ± 5
5	46.3 ± 1.2	65 ± 2	128 ± 3	43.6 ± 1.4	63 ± 2	126 ± 3	43.3 ± 1.7	62 ± 2	130 ± 3
6	41.3 ± 2.0	57 ± 2	136 ± 3	42.9 ± 0.4	58 ± 0	138 ± 2	41.7 ± 1.2	59 ± 1	132 ± 2
7	45.7 ± 1.3	63 ± 1	129 ± 5	46.5 ± 2.3	62 ± 2	134 ± 2	46.1 ± 1.6	62 ± 2	135 ± 2
8	45.2 ± 1.2	63 ± 1	130 ± 1	42.5 ± 0.5	62 ± 1	124 ± 3	42.8 ± 1.5	61 ± 0	129 ± 4
Average	45.7 ± 3.8	64 ± 4	126 ± 6	45.1 ± 3.3	64 ± 4	127 ± 8	45.0 ± 3.3	64 ± 4	127 ± 6

Summary of the reproducibility data. Global averages are given in the last row.

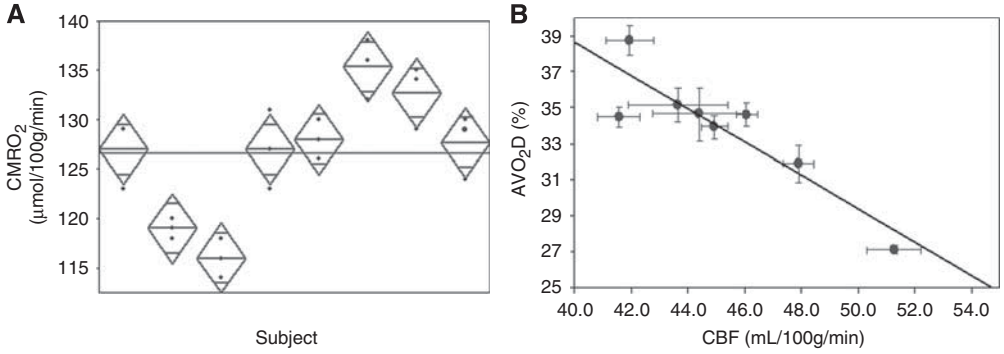

Figure 5 (**A**) Scatter plot of the cerebral metabolic rate of oxygen ($CMRO_2$) for each subject over three scanning sessions illustrating reproducibility. The vertical span of each diamond represents the 95% confidence interval (CI) for each group. (**B**) Correlation between AVO_2D and total cerebral blood flow (*CBF*) in the eight subjects ($R^2 = 0.74$, $P < 0.006$). Note that subjects with higher *CBF* values tend to have lower AVO_2D.

Discussion and Conclusion

We have introduced an MRI-based technique for quantifying absolute $CMRO_2$ in humans *in vivo*. The method is robust, reproducible, and allows for simultaneous measurement of oxygen saturation and flow rate. Our protocol takes around 3 minutes for whole-brain $CMRO_2$ quantification (including localizers), where the physiologically relevant S_vO_2 and blood flow estimation takes less than 30 seconds. The short acquisition times afforded by the technique make it suited for monitoring changes in $CMRO_2$ in response to physiologic challenges. The measured whole-brain $CMRO_2$ level averaged across the eight study subjects was 127 ± 7 μmol per 100 g per minute, which is in good agreement with the values reported in literature (Hattori *et al*, 2004; Ibaraki *et al*, 2008; Xu *et al*, 2009). Our results illustrate that the technique can estimate $CMRO_2$ with a high degree of precision and reliability (average coefficient of variation and intraclass correlation coefficient of 3.2% and 0.94, respectively). This level of precision is comparable to that reported using more invasive techniques. The strong correlation observed between the AVO_2D and global *CBF* is expected and has been reported earlier (Xu *et al*, 2009; Figure 5B). The intersubject variations in venous oxygen saturation, *CBF*, and $CMRO_2$ measurements were found to be statistically significant as compared with the intrasubject variations in these parameters (two-tailed analysis of variance, $P < 0.003$). These intersubject differences observed are physiologic and represent normal differences between subjects; the range seen is consistent with literature reports that have evaluated oxygen saturation and $CMRO_2$ levels using invasive methods such as jugular vein catheterization and positron emission tomography (Coles *et al*, 2002; Hattori *et al*, 2004; Nagdyman *et al*, 2005; Powers *et al*, 1985).

Other MRI-based approaches for the noninvasive quantification of blood oxygenation have resorted to measurements of the transverse relaxation times, T_2 and T_2^*, which are also related to the deoxyhemoglobin concentration in erythrocytes (Chien *et al*, 1994; Li *et al*, 1998; Wright *et al*, 1991). Unlike susceptometry-based oximetry, the sensitivity of T_2 and

T_2^*-based measurements varies with the level of hemoglobin oxygen saturation (both depend quadratically on HbO_2, although the relationship is piecewise linear over a small range of HbO_2 values; Chien *et al*, 1994; Li *et al*, 1998; Wright *et al*, 1991). The *in vivo* estimation of these parameters in the major blood vessels is complicated by body motion (requiring suspended respiration), pulsatile blood flow (necessitating cardiac gating), and the need for long pulse repetition times, leading to prolonged acquisition times (Li *et al*, 1998; Stainsby and Wright, 1998). The above factors make these methods less suited for measuring physiologic variations in $CMRO_2$ over experimental time frames as well as for clinical evaluations. Alternative approaches using positron emission tomography or Single Positron Emission Tomography (SPECT) (Frackowiak *et al*, 1980; Mintun *et al*, 1984) rely on contrast agents, are invasive (generally requiring arterial/venous lines for the administration of contrast agents), lengthy, and expensive.

Owing to the thin medial layer and lower distending pressure in veins, the SSS does not have a circular (or elliptic) cross-section as shown in Figure 4C. However, as $|\chi| \ll 1$, the induced field inside the vessel is parallel to the applied field (Schenck, 1996), and more importantly, the effect of cross-sectional geometry is negligible as long as the vessel is parallel to the applied field. In our study, the SSS, used for S_vO_2 measurement, was essentially parallel to B_o (average tilt angle across subjects $<6^\circ$) and has negligible curvature at the measurement site (Figures 4A and 4B). The above predictions are supported by our phantom experiments (Figure 2; Table 1), consisting of test tubes with triangular and circular cross-section filled with varying Gd-DTPA-doped water concentrations positioned parallel to B_o. The uniform phase accumulation inside the triangular tubes, the clear phase separation from the surrounding distilled water, and strong agreement with the susceptibility measurement in the circular tubes lend strong support to the validity of the model adopted in this work. The largest relative difference in measured susceptibility between tubes of circular and triangular cross-section was less than 5%, which translates to a difference of less than 2% HbO_2. In keeping with the requirements for applicability of the model, the SSS also complies with the long cylinder approximation. Previous work has shown that a length to diameter ratio of ~ 6 is sufficient to apply the long cylinder model (Langham *et al*, 2009*b*). Posteriorly, the typical sagittal sinus segment has length to diameter ratios of >6 (typical vessel diameter $\sim$5 to 6 mm; vessel segment length $\sim$4 cm; Figures 4A and 4B).

Finally, a few constants prone to intersubject variability and used in the estimation of $CMRO_2$ can be additional sources of error. A typical *Hct* value of 42% was used for all our measurements. We expect that the variation in hematocrit within our study cohort is minimal (all males, age: 25 ± 5 years) and could be obtained by blood draws. A typical S_aO_2 value of 98% was used for all the calculations. Although this value is widely accepted in literature, an accurate measurement of S_aO_2 can easily be obtained at a different site where an artery is present.

The present technique estimates global $CMRO_2$ but not regional. All previously explored methods for regional $CMRO_2$ quantification are model based and are still in their developmental stages. One such approach relies on the estimation of the contribution to the effective transverse relaxation rate from regional magnetic field inhomogeneity ($T2'$) resulting from partially desaturated blood in the capillary bed. From this quantity, along with a measurement of capillary volume, the oxygen extraction fraction is derived (An and Lin, 2003; He and Yablonskiy, 2007). Nonetheless, the importance of a global measure to estimate absolute cerebral metabolism is of interest in its own right.

In conclusion, we have shown a noninvasive MRI-based approach for the estimation of global whole-brain $CMRO_2$ based on simultaneous measurement of average blood flow rate and oxygen saturation in major inflow and outflow vessels to the brain. The noninvasive nature of the technique, its robustness, and straightforward implementation make it suitable for applications in clinical settings for the assessment of pathologies associated with disorders of brain metabolism. Rapid acquisition afforded by the technique makes it specially suited for studying temporal variations in $CMRO_2$ under physiologic challenges such as hypercapnia, hyperoxia, caffeine stimulation, and sedation, as well as under functional brain paradigms.

Disclosure/conflict of interest

The authors declare no conflict of interest.

References

Abduljalil AM, Schmalbrock P, Novak V, Chakeres DW (2003) Enhanced gray and white matter contrast of phase susceptibility-weighted images in ultra-high-field magnetic resonance imaging. *J Magn Reson Imaging* 18:284–90

An H, Lin W (2003) Impact of intravascular signal on quantitative measures of cerebral oxygen extraction and blood volume under normo- and hypercapnic conditions using an asymmetric spin echo approach. *Magn Reson Med* 50:708–16

Bryant DJ, Payne JA, Firmin DN, Longmore DB (1984) Measurement of flow with NMR imaging using a gradient pulse and phase difference technique. *J Comput Assist Tomogr* 8:588–93

Chien D, Levin DL, Anderson CM (1994) MR gradient echo imaging of intravascular blood oxygenation: T2* determination in the presence of flow. *Magn Reson Med* 32:540–5

Coles JP, Minhas PS, Fryer TD, Smielewski P, Aigbirihio F, Donovan T, Downey SP, Williams G, Chatfield D, Matthews JC, Gupta AK, Carpenter TA, Clark JC, Pickard

JD, Menon DK (2002) Effect of hyperventilation on cerebral blood flow in traumatic head injury: clinical relevance and monitoring correlates. *Crit Care Med* 30:1950–9

Cooper ER (1960) The vertebral venous plexus. *Acta Anat (Basel)* 42:333–51

Coplin WM, O'Keefe GE, Grady MS, Grant GA, March KS, Winn HR, Lam AM (1997) Thrombotic, infectious, and procedural complications of the jugular bulb catheter in the intensive care unit. *Neurosurgery* 41:101–7; discussion 107–9

Dumoulin CL, Hart HR, Jr (1986) Magnetic resonance angiography. *Radiology* 161:717–20

Fernandez-Seara MA, Techawiboonwong A, Detre JA, Wehrli FW (2006) MR susceptometry for measuring global brain oxygen extraction. *Magn Reson Med* 55:967–73

Frackowiak RS, Lenzi GL, Jones T, Heather JD (1980) Quantitative measurement of regional cerebral blood flow and oxygen metabolism in man using 15O and positron emission tomography: theory, procedure, and normal values. *J Comput Assist Tomogr* 4:727–36

Greene AE, Todorova MT, Seyfried TN (2003) Perspectives on the metabolic management of epilepsy through dietary reduction of glucose and elevation of ketone bodies. *J Neurochem* 86:529–37

Haacke EM, Lai S, Reichenbach JR, Kuppusamy K, Hoogenraad FGC, Takeichi H, Lin W (1997) *In vivo* measurement of blood oxygen saturation using magnetic resonance imaging: a direct validation of the blood oxygen level-dependent concept in functional brain imaging. *Hum Brain Mapp* 5:341–6

Hattori N, Bergsneider M, Wu HM, Glenn TC, Vespa PM, Hovda DA, Phelps ME, Huang SC (2004) Accuracy of a method using short inhalation of (15)O-O(2) for measuring cerebral oxygen extraction fraction with PET in healthy humans. *J Nucl Med* 45:765–70

He X, Yablonskiy DA (2007) Quantitative BOLD: mapping of human cerebral deoxygenated blood volume and oxygen extraction fraction: default state. *Magn Reson Med* 57:115–26

Ibaraki M, Miura S, Shimosegawa E, Sugawara S, Mizuta T, Ishikawa A, Amano M (2008) Quantification of cerebral blood flow and oxygen metabolism with 3-dimensional PET and 15O: validation by comparison with 2-dimensional PET. *J Nucl Med* 49:50–9

Ishii K, Kitagaki H, Kono M, Mori E (1996) Decreased medial temporal oxygen metabolism in Alzheimer's disease shown by PET. *J Nucl Med* 37:1159–65

Ito H, Ibaraki M, Kanno I, Fukuda H, Miura S (2005) Changes in cerebral blood flow and cerebral oxygen metabolism during neural activation measured by positron emission tomography: comparison with blood oxygenation level-dependent contrast measured by functional magnetic resonance imaging. *J Cereb Blood Flow Metab* 25:371–7

Kety SS, Schmidt CF (1948) The effects of altered arterial tensions of carbon dioxide and oxygen on cerebral blood flow and cerebral oxygen consumption of normal young men. *J Clin Invest* 27:484–92

Kretschmann HJ, Kammradt G, Krauthausen I, Sauer B, Wingert F (1986) Brain growth in man. *Bibl Anat* 28: 1–26

Langham MC, Magland JF, Epstein CL, Floyd TF, Wehrli FW (2009*b*) Accuracy and precision of MR blood oximetry based on the long paramagnetic cylinder approximation of large vessels. *Magn Reson Med* 62:333–40

Langham MC, Magland JF, Floyd TF, Wehrli FW (2009*a*) Retrospective correction for induced magnetic field inhomogeneity in measurements of large-vessel hemoglobin oxygen saturation by MR susceptometry. *Magn Reson Med* 61:626–33

Leenders KL, Frackowiak RS, Quinn N, Marsden CD (1986) Brain energy metabolism and dopaminergic function in Huntington's disease measured *in vivo* using positron emission tomography. *Mov Disord* 1:69–77

Li D, Wang Y, Waight DJ (1998) Blood oxygen saturation assessment *in vivo* using T2* estimation. *Magn Reson Med* 39:685–90

Lowry OH, Passonneau JV, Hasselberger FX, Schulz DW (1964) Effect of ischemia on known substrates and cofactors of the glycolytic pathway in brain. *J Biol Chem* 239:18–30

Lu H, Ge Y (2008) Quantitative evaluation of oxygenation in venous vessels using T2-relaxation-under-spin-tagging MRI. *Magn Reson Med* 60:357–63

Magistretti PJ, Pellerin L (1996) Cellular mechanisms of brain energy metabolism. Relevance to functional brain imaging and to neurodegenerative disorders. *Ann N Y Acad Sci* 777:380–7

Magland J, Wehrli F (2006) Pulse sequence programming in a dynamic visual environment. In: *Proceedings of the 14th Annual Meeting of ISMRM* Seattle, WA (Abstract 578)

Mayberg TS, Lam AM (1996) Jugular bulb oximetry for the monitoring of cerebral blood flow and metabolism. *Neurosurg Clin N Am* 7:755–65

Mintun MA, Raichle ME, Martin WR, Herscovitch P (1984) Brain oxygen utilization measured with O-15 radiotracers and positron emission tomography. *J Nucl Med* 25:177–87

Mugler JP, III, Brookeman JR (1990) Three-dimensional magnetization-prepared rapid gradient-echo imaging (3D MP RAGE). *Magn Reson Med* 15:152–7

Nagdyman N, Fleck T, Schubert S, Ewert P, Peters B, Lange PE, Abdul-Khaliq H (2005) Comparison between cerebral tissue oxygenation index measured by near-infrared spectroscopy and venous jugular bulb saturation in children. *Intensive Care Med* 31:846–50

Pelc NJ, Sommer FG, Li KC, Brosnan TJ, Herfkens RJ, Enzmann DR (1994) Quantitative magnetic resonance flow imaging. *Magn Reson Q* 10:125–47

Playvin YA, Blum EY (1983) Magnetic parameters of blood cells and high gradient paramagnetic and diamagnetic phoresis. *Magnitnaya Gidrodinamika* 19:3–15

Powers WJ, Grubb RL, Jr, Darriet D, Raichle ME (1985) Cerebral blood flow and cerebral metabolic rate of oxygen requirements for cerebral function and viability in humans. *J Cereb Blood Flow Metab* 5:600–8

Quastel JH, Wheatley AH (1932) Oxidations by the brain. *Biochem J* 26:725–44

Santens P, De Reuck J, Crevits L, Decoo D, Lemahieu I, Strijckmans K, Goethals P (1997) Cerebral oxygen metabolism in patients with progressive supranuclear palsy: a positron emission tomography study. *Eur Neurol* 37:18–22

Schenck JF (1996) The role of magnetic susceptibility in magnetic resonance imaging: MRI magnetic compatibility of the first and second kinds. *Med Phys* 23:815–50

Shishido F, Uemura K, Inugami A, Tomura N, Higano S, Fujita H, Sasaki H, Kanno I, Murakami M, Watahiki Y, Nagata K (1996) Cerebral oxygen and glucose metabolism and blood flow in mitochondrial encephalomyopathy: a PET study. *Neuroradiology* 38:102–7

Spees WM, Yablonskiy DA, Oswood MC, Ackerman JJ (2001) Water proton MR properties of human blood at 1.5 Tesla: magnetic susceptibility, T(1), T(2), T*(2), and non-Lorentzian signal behavior. *Magn Reson Med* 45:533–42

Stainsby JA, Wright GA (1998) Partial volume effects on vascular T2 measurements. *Magn Reson Med* 40:494–9

Tanaka M, Kondo S, Okamoto K, Hirai S (1997) Cerebral perfusion and oxygen metabolism in Parkinson's disease: positron emission tomographic study using oxygen-15-labeled CO2 and O2. *Nippon Rinsho* 55:218–21

Thulborn KR, Waterton JC, Matthews PM, Radda GK (1982) Oxygenation dependence of the transverse relaxation time of water protons in whole blood at high field. *Biochim Biophys Acta* 714:265–70

Weisskoff RM, Kiihne S (1992) MRI susceptometry: image-based measurement of absolute susceptibility of MR contrast agents and human blood. *Magn Reson Med* 24:375–83

West JB (2007) *Pulmonary physiology and pathophysiology: an integrated, case-based approach*. 2nd ed. Philadelphia, PA: Lippincott Williams & Wilkins

Wright GA, Hu BS, Macovski A (1991) 1991 I.I. Rabi Award. Estimating oxygen saturation of blood *in vivo* with MR imaging at 1.5 T. *J Magn Reson Imaging* 1: 275–83

Xu F, Ge Y, Lu H (2009) Noninvasive quantification of whole-brain cerebral metabolic rate of oxygen (CMRO2) by MRI. *Magn Reson Med* 62:141–8

Yushkevich PA, Piven J, Hazlett HC, Smith RG, Ho S, Gee JC, Gerig G (2006) User-guided 3D active contour segmentation of anatomical structures: significantly improved efficiency and reliability. *Neuroimage* 31:1116–28